Simulation of a full ISRU-based system for energy storage and electricity generation on the Moon

F. Palos, Mario, Stephenson, Keith**, and González-Cinca, Ricard****
**Department of Physics, UPC-BarcelonaTech*
C/ E. Terradas 5, 08860 Castelldefels (Barcelona), Spain,
Email: mario.fernandez.palos@upc.edu
***European Space Agency, ESTEC TEC-EPM*
Keplerlaan 1, 2201AZ Noordwijk (The Netherlands)
Email: keith.stephenson@esa.int
****Department of Physics, UPC-BarcelonaTech*
C/ E. Terradas 5, 08860 Castelldefels (Barcelona), Spain
Email: ricard.gonzalez@upc.edu

Abstract

The survival of the crew and assets during the lunar night is one of the biggest challenges in the exploration of the Moon. The storage and supply of energy are key elements for the success of a mission. We present numerical simulations of a system based on ISRU that stores solar energy during the day and generates electricity during the night. We carried out analyses of each subsystem as well as simulations of the full system. Estimates of the performance of the system in terms of power output and mass of the system are presented.

1. Introduction

Exploring the lunar surface is a key target in the human and robotic space exploration plans of space agencies. The survival of the crew and lunar assets is one of the biggest challenges in the exploration of the Moon. The day/night cycle, with long periods of darkness, and the environmental conditions of the lunar surface, make the storage and provision of energy a critical challenge. A system to store heat and generate electricity consisting of mirrors, processed lunar soil and a heat engine has been proposed to provide energy to vehicles and crew during the lunar night [1, 2]. During the lunar day, the system can run the engine directly using the solar power and simultaneously heat an ISRU-based thermal mass. This thermal mass is used as a high temperature source to run the heat engine during the night. The system is scalable and can be applicable to all regions of the Moon and in other exploration environments.

In this work we present a computer model of the lunar ISRU energy storage and electrical generation system. Individual analyses of each subsystem, and simulation of the full system are presented. Estimates of the performance of the system in terms of power/energy output, mass of the system, etc. are also discussed.

2. Model

The system architecture presented in [2] is the base of the used model. Figure 1 shows a 3D representation of the system, which is composed of the following elements: mirror field, receiver tube, thermal mass, heat engine, and radiator with sunshield.

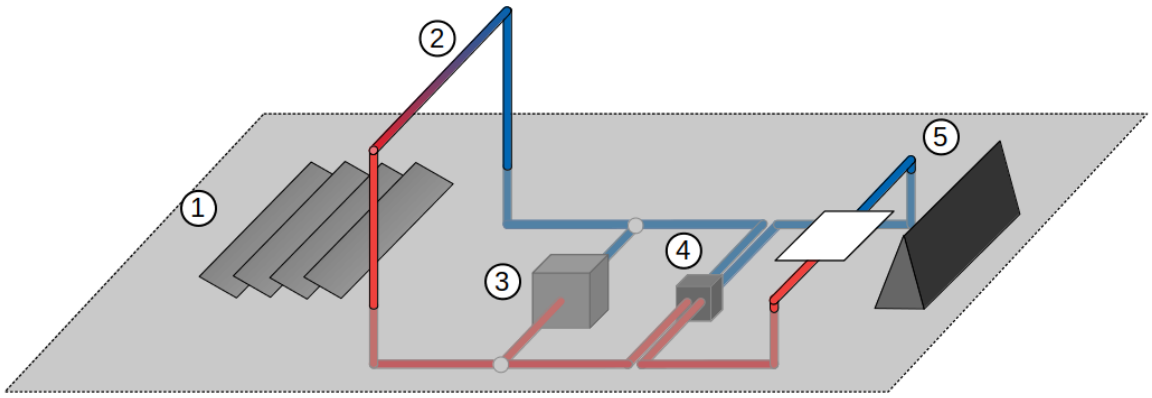

Figure 1: Sketch of the system: (1) Mirror field, (2) Receiver tube, (3) Thermal mass, (4) Heat engine, (5) Radiator with sunshield.

The system contains three fluid loops. The collection loop runs during the lunar day, transferring heat from the sunlight collector to the thermal mass and rising its temperature. The discharge loop is active during the lunar night, transferring heat from the thermal mass to the hot side of the heat engine. The radiator loop runs when the heat engine is running, transferring heat from the cold side of the heat engine to the radiator. In addition to the main components, the system includes some extra elements: valves, pumps, and two expansion tanks to control pressure. Figure 2 shows a simplified diagram of the system main components and connections, and of the direction of the flows.

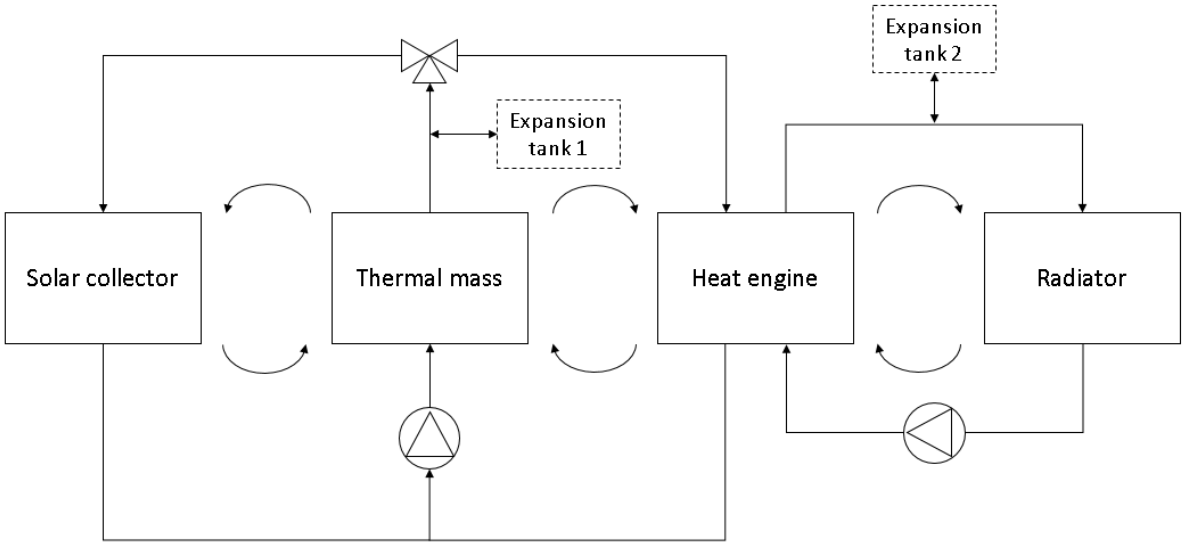

Figure 2: Simplified diagram of the system and heat flow.

The system model built in EcosimPro contains some components obtained from the additional library Fluidapro, while others were obtained from default libraries or were custom made. Subsystems models were initially simulated individually for validation. Later all subsystems were integrated into the full system model. All subsystems represent parts of the full system on the surface of the Moon with lunar gravity (except during validation tests).

3. Subsystems

3.1 Solar energy collector

Figure 3 shows the model of the solar energy or sunlight collection subsystem, which represents the collection of solar power by the mirror field and the collection loop. The model consists of a mirror field that directs sunlight into an elevated structure (the receiver). Sunlight is focused in the receiver tube, which transports the working fluid.

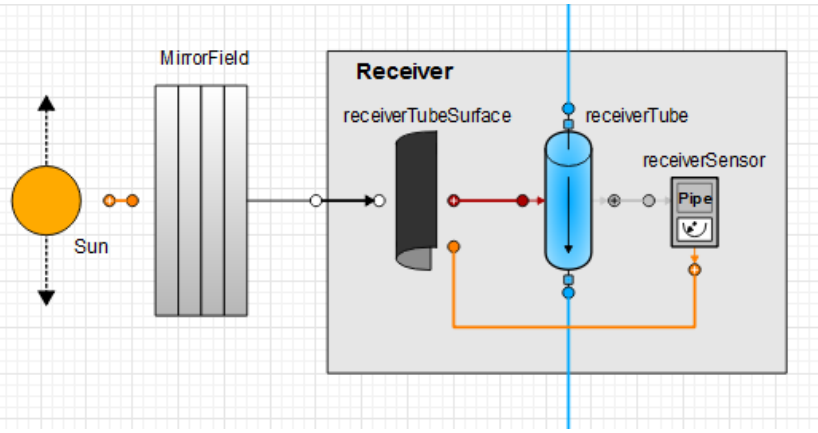

Figure 3: Solar energy collection subsystem.

Table 1 shows the values used in the solar collection subsystem in the simulation.

Table 1: Characteristics of the solar energy collection components.

Mirror field	
Concentration ratio	100
Mirror area (m^2)	500
Receiver	
Area width (m)	0.5
Area length (m)	10
Pipe width (m)	0.01

3.2 Energy storage

Figure 4 shows the model of the energy storage subsystem. The model represents a cylindrical thermal mass (10 m length and 1 m external diameter), made of sintered regolith with a tube in the middle. The heat transfer fluid (HTF) flows through the tube, exchanging heat with the mass by conduction. The choice of a cylinder instead of a rectangular prism, which could be more appropriate for stacking several tubes in parallel, is based on the fact that solid cylinders made of custom materials are available in EcosimPro by default.

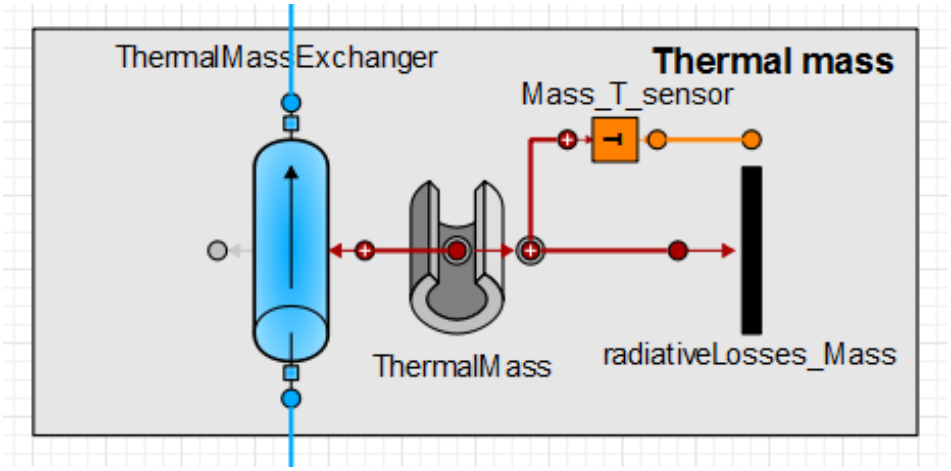

Figure 4: Energy storage subsystem.

The trade-off results called for the inclusion of thermal fins, this is, metallic plates connected to the tube and penetrating into the thermal mass in order to improve conduction. Simulations show that fins are not necessary since temperature inside the mass reaches a steady state at the considered times (see results further).

The mass is buried underground and surrounded by a vacuum layer, except for the required structural supports. Therefore, most of the energy losses to the environment are caused by radiation. The surrounding native regolith is at 273 K. Neither thermal variations of temperature during the lunar day and night nor any increase in temperature due to the presence of the discharging thermal mass are taken into account.

Table 2 shows the characteristics of the subsystem in the model. The size of the thermal mass, made of sintered regolith, has been chosen so that it can be completely recharged during daytime. Table 3 shows the properties of the sintered regolith.

Table 2: Characteristics of the energy storage components.

Tube	
Length (m)	10
Diameter (m)	0.01
Thermal mass	
Length (m)	10
Internal diameter (m)	0.01
External diameter (m)	1
Volume of material (m^3)	7.85
Material	Sint. regolith

Table 3: Properties of the sintered regolith.

Density (kg/m^3)	3000
Specific heat (J/(kg K))	800
Thermal conductivity (W/(m K))	22.1

3.3 Heat transport

The heat transport subsystem represents the circuit through which the HTF flows. Aside from the pipes, this subsystem includes additional components like valves, check valves, pumps, and structural supports. The diameter of the pipes is the same as the diameter of the tubes inside the thermal mass (see Table 2). The two main components of the heat transport subsystem are the HTF and the pressure control of the fluid.

Figure 5 shows the pressure control unit located in two positions in the system. One unit is located in the shared branch between the collection loop and the discharge loop, and the other unit is in the radiator loop. Their mission is to act as expansion tanks for any possible increase in volume that may occur in the HTF, and also to impose a boundary condition for the pressure.

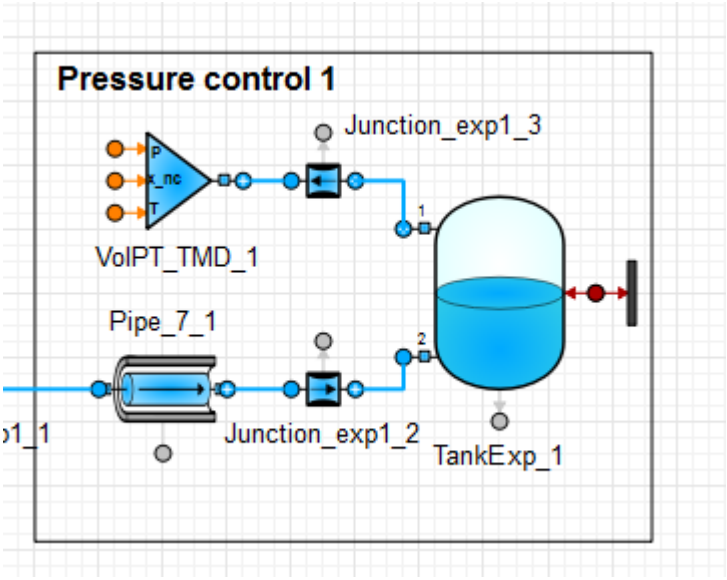

Figure 5: Pressure control unit.

The two pressure control units have the same components, the only difference being the pressure imposed on each one. The collection and discharge loops are limited to 1 MPa, while the radiator loop is kept at 0.1 MPa. The units are composed of an expansion tank, situated above the circuit, and connected to the pressure condition. The use of bladder tanks with an additional gas pressurizing the liquid was considered, but it increased the simulation times while providing no apparent advantage.

The nature of the system and the condition of the missions seem to ask for thermal mass temperatures as high as possible, in order to ensure high enough end-of-night (EON) temperatures to feed the heat engine. For this it is necessary to develop a custom HTF, as the liquids available by default in EcosimPro's Fluidapro have relatively low boiling points. Lu *et al.* [3] suggested using liquid metals (liquid sodium, in particular) or molten salts (nitrate) for high-temperature lunar applications. Lorenzin *et al.* [4] concluded that liquid metals are a better choice than molten salts, proposing liquid sodium and liquid lithium. Both liquids are used nowadays as HTFs in nuclear reactors, mostly in naval nuclear engines.

Simulating liquids in EcosimPro with their liquid and gaseous properties has proven to be very challenging. However, if the system uses liquid metal as the HTF, it should not vaporize at any moment. This opens up the possibility of including only the liquid properties, and keeping an eye on the fluid to check that it never vaporizes. The fluid temperature cannot be above the saturation temperature at the given pressure.

The HFT used in the simulations is liquid sodium (critical temperature of 2573 K). Liquid sodium is one of the few HTFs that could remain in liquid phase in the complete range of temperatures, avoiding the extra complications of simulating and operating two-phase flows. Even if the data for the vapor pressure is included in the model, EcosimPro does not use them because it works under the assumption that the HFT is always in liquid phase. Temperature and pressure values are manually checked in order to make sure that no evaporation occurs at any point in the liquid.

3.4 Heat-to-electricity conversion

Heat engines stand out among the other options for heat-to-electricity conversion [2]. Simulating the internal details of the heat engine was not considered from the start, since such a simulation could become as complex as the simulation of the full power system without the engine. Hence, the power generated for a given temperature difference is not provided. Instead, a different approach is carried out. The simulator provides a heat flow to the engine hot side, and outputs a fraction of it as electrical power according to a given efficiency, releasing the rest of the heat to the radiator circuit from the cold side of the engine. This approach provides an upper limit to the amount of power that the system can generate, regardless of the heat engine used.

Figure 6 shows the model of the heat-to-electricity subsystem, which consists of the custom component heat engine located between two default EcosimPro tubes, acting as the heat exchangers of the hot and cold sides of the heat engine.

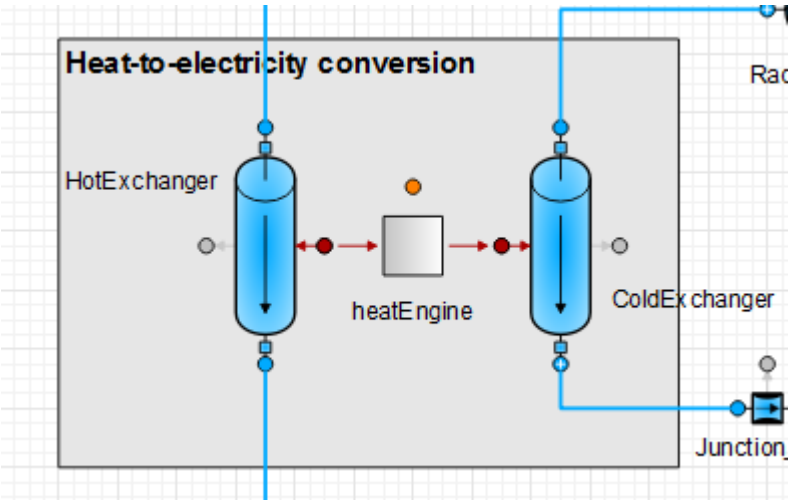

Figure 6: Heat-to-electricity conversion subsystem.

3.5 Heat rejection

Figure 7 shows the model of the heat rejection subsystem consisting of a fluid loop, separated from the main one, with the radiator, a fluid pump and a pressure control system. Ethanol is used as HTF. The circuit transfers heat from the cold side of the engine to the radiator, which is connected to a component simulating the environment temperature of 4 K. EcosimPro includes the model of a radiator that fits the needs of the system. The radiator is made of a metal with a customizable geometry and crossed by fluid pipes. In the current model the radiator consists of two fins made of aluminum. Fins are 3 m wide and 13 m long, which corresponds to the approximate size of one radiator of the International Space Station [5]. The radiating area taking into account both sides is approximately 78 m^2. This is an oversized radiator for such a small thermal mass, but the choice of this radiator is related to the difficulties in optimizing the radiator circuit.

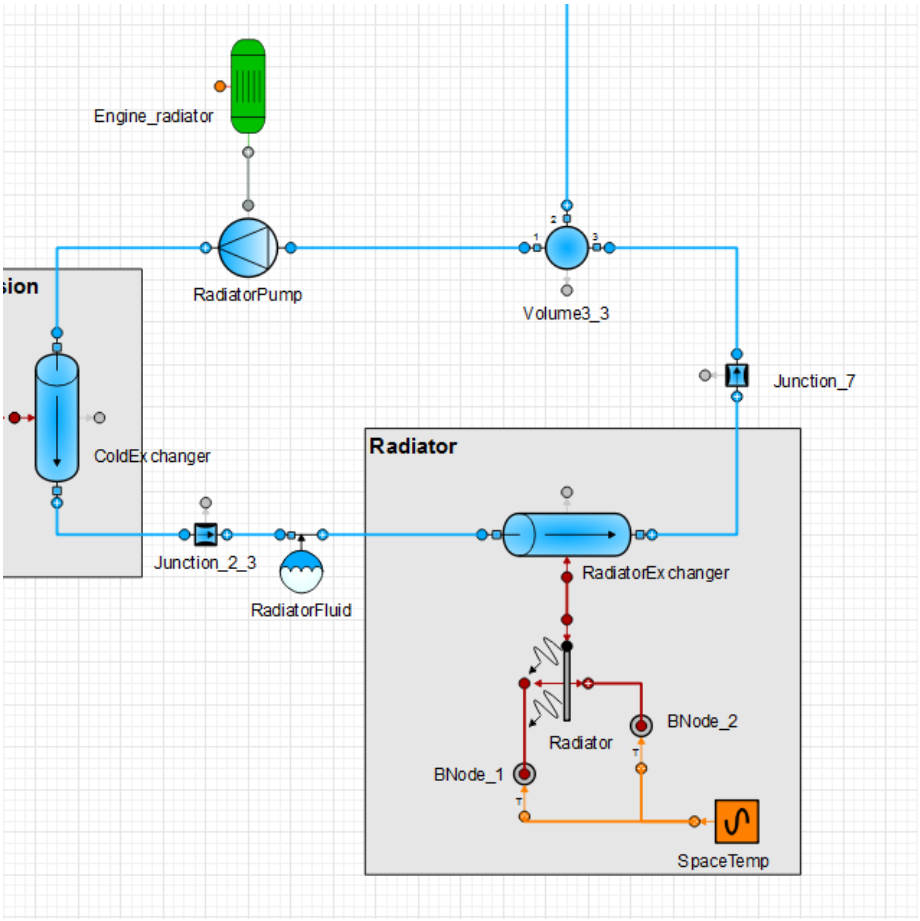

Figure 7: Heat rejection subsystem.

4. Full system analysis

Simulations of the full system model were carried out in order to analyze its performance.

Figure 8 shows the temperature reached by the HTF in the receiver during a lunar day. The temperature does not follow the sinusoidal pattern that the Sun follows in the model, but instead reaches a stable temperature of 1600 K for half of the lunar day. This behavior is due to the fact that the black-body radiation scales very rapidly with temperature.

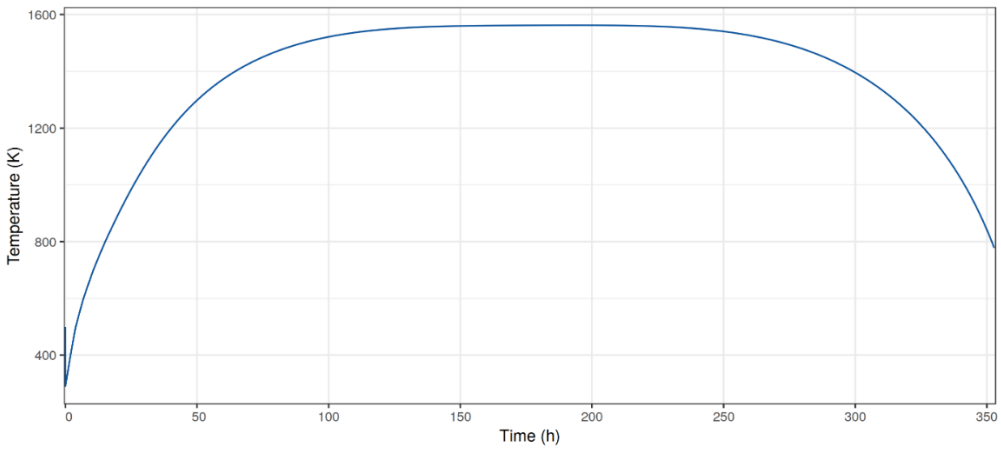

Figure 8: Temperature of the HTF in the receiver between sunrise and sunset.

Figure 9 shows the temperature of the thermal mass during charge, measured in five different radial nodes. The temperature in the inner node (T1) is the one that reacts fastest to the change, while the one at the outer node (T5) has the slowest reaction. When sunset starts (around 270 h or 1e+06 s) a thermal gradient decreasing outwards is in the thermal mass. The decrease of the temperature after sunset is due to the lower solar illumination.

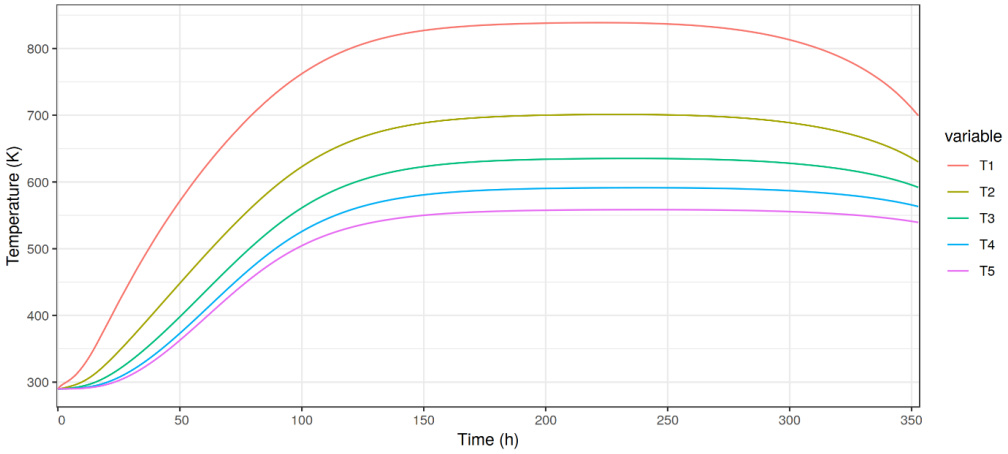

Figure 9: Thermal mass temperature during charge.

.

Figure 10 shows the temperature of the thermal mass in the discharge phase during a lunar night while the heat engine is disconnected. Heat is lost through radiation of the outer most layer, and the EON temperature is in this case approximately 355 K.

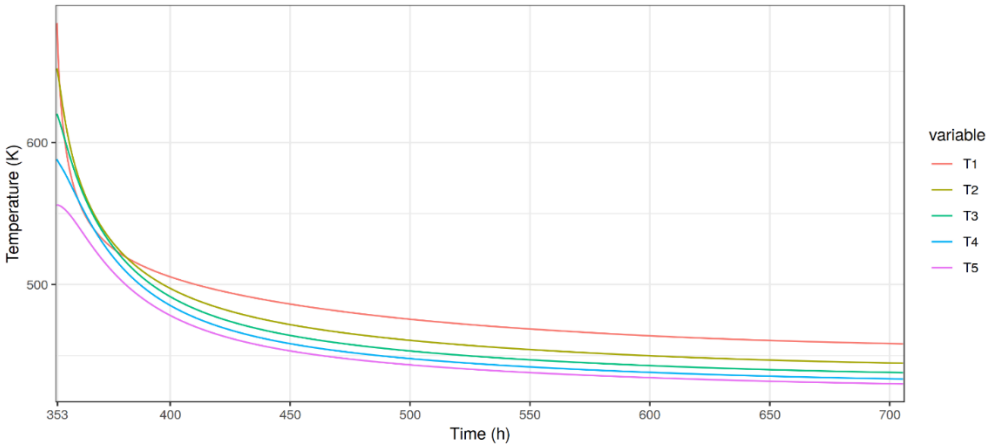

Figure 10: Thermal mass temperature during discharge.

In order to determine the electrical power generated by the system, the following considerations have been taken into account: i) the EON temperature of the thermal mass has to be sufficiently high to power the heat engine, ii) the charge-discharge cycle has to be able to reach a full recharge during the day.

Figure 11 shows the evolution of the temperature of the thermal mass during the night while 1000 W are provided to the heat engine, which results in 100 We for a heat engine of 10% efficiency. The behavior of the temperature is very similar to the case with a disconnected heat engine (Figure 10), except for the lower EON temperature in the case with the connected heat engine. We can conclude that thermal losses by radiation play an important role in the thermal mass temperature. Therefore, a reduction of thermal losses by radiation could significantly improve the performance of the system.

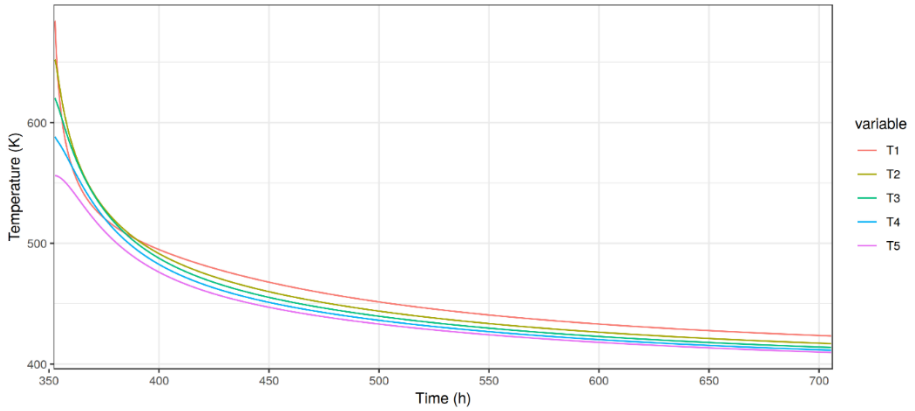

Figure 11: Discharge of the thermal mass during the night with the heat engine connected.

Figure 12 shows the temperature in the heat exchanger on the hot and cold sides of the heat engine, which is associated to the thermal gradient in the engine. According to Figure 9, the thermal mass takes about $1.5 \cdot 10^6$ seconds to reach the equilibrium temperature starting from ~300 K. Therefore, it will be able to reach these conditions after being connected to the heat engine during the night.

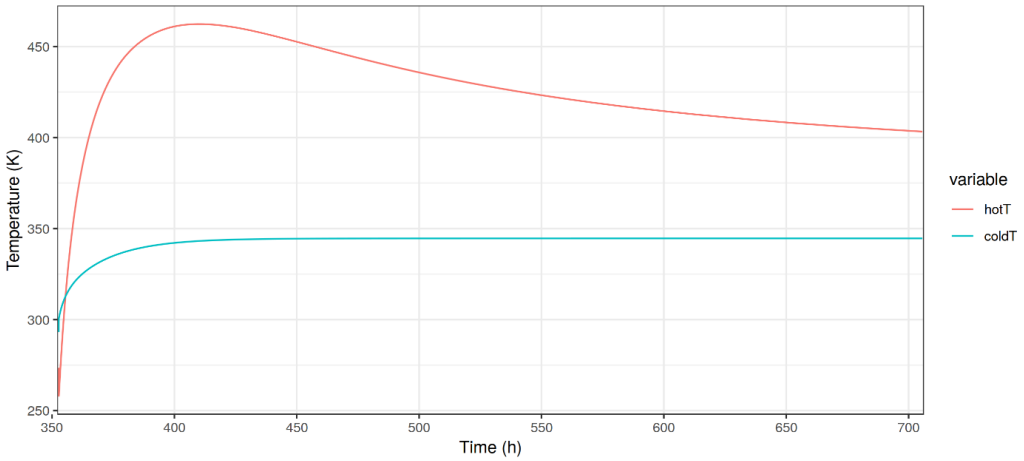

Figure 12: Temperature of the cold and hot sides of the heat engine.

Figure 13 shows the effect of the efficiency of the heat engine in the temperature of the inner node of the thermal mass for a power output of 100 We. A higher efficiency implies a smaller amount of heat taken from the discharge loop, resulting in a smaller decrease of the temperature.

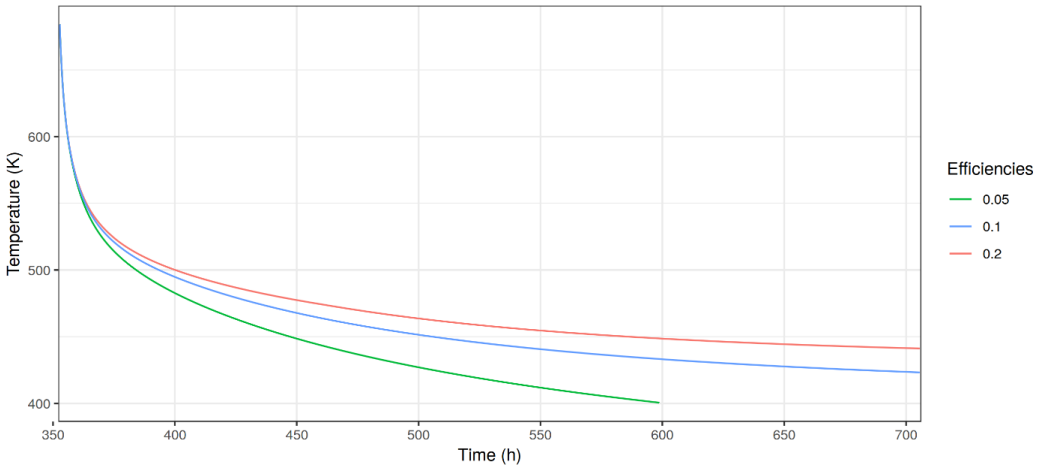

Figure 13: Effect of engine efficiency on the discharge of the thermal mass.

The structure of the simulator does not allow to open the collection and discharging loops at the same time, hence the power generation during daytime cannot be directly shown. However, it is possible to get a glimpse of it by adding the thermal power that would be normally extracted (1000 W, in order to generate 10 We) to the power lost by the thermal mass in the form of radiation (Figure 14). The effect is not completely realistic, as the radiated power is lost through the external surface, while the power given to the engine would come from the inner surface. However, it can be observed that the temperature at the end of the day is only about 5 K lower than in Figure 9. This is an expected behavior, as power losses in the mass are far greater than the power consumption of the heat engine.

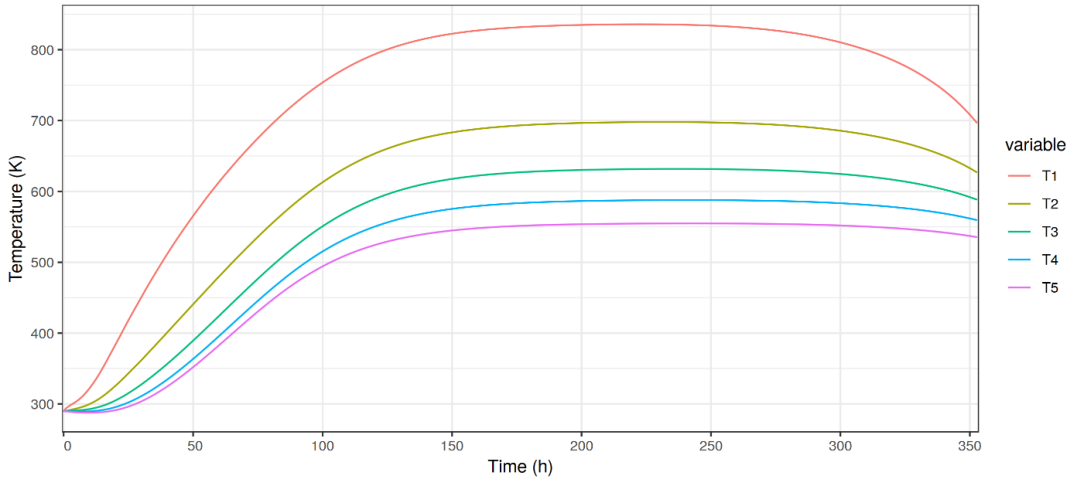

Figure 14: Thermal mass charging with 1000 W extra lost to radiation.

Figure 15 shows the time evolution of the temperature on the five axial nodes of the heat exchanger with the radiator. The temperature decreases as the HFT travels farther along the tube from T1 to T5. The temperature quickly reaches a steady state as a consequence of the equilibrium between the heat coming from the heat engine and the heat radiated into space.

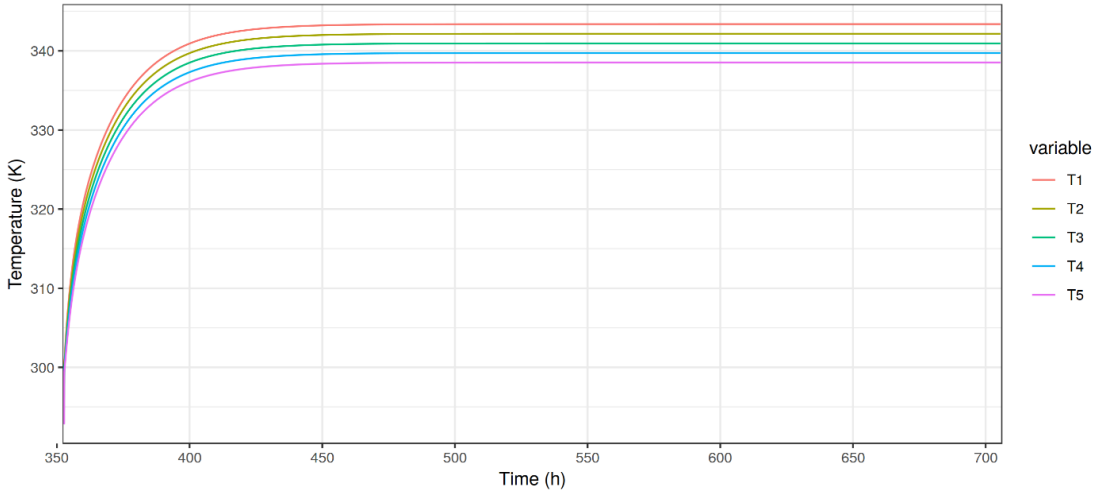

Figure 15: Temperature on the axial nodes of the radiator thermal exchanger during the night

5. Discussion and conclusions

In order to analyze the feasibility of the system, the specific power is calculated in two scenarios. In the first one, the characteristics of the components corresponding to simulations to generate 100 We are considered. In the second scenario, an estimation of the specific power for a larger system that can generate 10 kWe has been carried out.

The estimated total mass of the components for the 100 We scenario is 25054.54 kg with the ISRU thermal mass, and 1454.54 kg without taking it into account. Therefore, for a power generation of 100 We, the specific power of the total

system would be $0.40 \cdot 10^{-2}$ W·kg^{-1}. Leaving the thermal mass out and considering only the mass required to be brought from Earth, the value goes up to 0.069 W·kg^{-1}.

The estimated total mass of the components for the 10 kWe scenario is $2.38 \cdot 10^{6}$ kg with the ISRU mass, and 18918.78 kg without it. The final specific power would be $4.2 \cdot 10^{-3}$ W·kg^{-1} with the thermal mass, and 5.29 W·kg^{-1} without taking it into account.

If in the future there was a chance to make mirrors out of ISRU materials, or by reusing materials from visiting spacecraft in order to save weight, the required mass could be significantly reduced.

Table 4 summarize the results for the two considered configurations of power supply.

Table 4: Mass and specific mass of the different configurations.

Power (We)	Total mass (kg)	Total mass, no ISRU (kg)	Specific mass, total system (W·kg^{-1})	Specific mass, no ISRU (W·kg^{-1})
100	$2.51 \cdot 10^{4}$	$1.45 \cdot 10^{3}$	$0.40 \cdot 10^{-2}$	0.069
10^{4}	$2.38 \cdot 10^{6}$	$1.89 \cdot 10^{4}$	$0.42 \cdot 10^{-2}$	0.53

These results could be compared to those of the technology that this system aims to beat in this scenario: photovoltaic power plus batteries. As a reference we can use the Li-ion batteries that have been recently installed on the ISS. These batteries are contained in boxes called Orbital Replacement Units (ORUs) that include not only the power cells, but also all the necessary connections, controllers, and safety components. It is expected that batteries would be delivered to the Moon in a similar configuration, in containers of specified size and connections, that are protected from launch stresses and vacuum environment, and are easy to replace when necessary. A difference that one can think of between the requirements of the orbit and the lunar surface may be in the amount of protection from micrometeoroids. The battery ORUs could be protected by the lunar surface, or by 3D printed structures. In order to account for that, we can substract some weight from the calculations.

Each Li-ion battery ORU weighs 197.3 kg [6], that we can reduce to 150 kg in order to account for the removal of micrometeoroid protection. Each ORU contains 30 cells connected in series, each with a nominal capacity of 148 Ah and a nominal voltage of 3.7 V. This gives an energy of 548 Wh per cell, or 16.44 kWh for a complete ORU. In order to hold enough energy for a lunar night (3.54e+6 Wh), it would be necessary to have 215 ORUs, that would weigh 32250 kg. This value is considerably larger than the mass of the ISRU-based system excluding the thermal mass (18918.78 kg). In addition, the mass of the additional components required (connections, controllers, and solar panels) has not been taken into account in the calculation.

In conclusion, the estimation of the mass required to supply 10 kWe by the ISRU-based thermal energy storage and electricity generation system shows that this system is very competitive in comparison to a system composed of photovoltaic panels and batteries.

Acknowledgements

This work was financially supported by the European Space Agency (ESA) through contract 4000124000/18/NL/AF.

References

[1] B. Climent, O. Torroba, R. González-Cinca, N. Ramachandran, M.D. Griffin, Heat storage and electricity generation in the Moon during the lunar night, *Acta Astronautica* 93, 352 (2014).
[2] M.F. Palos, P. Serra. S. Fereres, K. Stephenson, R. González-Cinca, Lunar ISRU energy storage and electricity generation, *Acta Astronautica* 170, 412 (2020).
[3] X. Lu, R. Ma, C. Wang and W. Yao, Performance analysis of a lunar based solar thermal power system with regolith thermal storage, *Energy* 107, 227 – 233 (2016).
[4] N. Lorenzin and A. Abánades, A review on the application of liquid metals as heat transfer fluid in Concentrated Solar Power technologies, *International Journal of Hydrogen Energy*, Vols. I-6 (2016).
[5] A. J. Hanford and M. K. Ewert, Advanced Active Thermal Control Systems Architecture Study, NASA (1996).
[6] P. J. Dalton. [Online]. Available: https://ntrs.nasa.gov/search.jsp?R=20170004524.